Vacuum-ultraviolet spectroscopy and quantum cutting for Gd^{3+} in $LiYF_4$

R. T. Wegh,* H. Donker, and A. Meijerink
Debye Institute, Utrecht University, P.O. Box 80 000, 3508 TA Utrecht, The Netherlands

R. J. Lamminmäki and J. Hölsä
Department of Chemistry, University of Turku, FIN-20014 Turku, Finland

(Received 27 March 1997)

A systematic spectroscopic study of the $4f^7$ energy levels of Gd^{3+} in $LiYF_4$ in the vacuum-ultraviolet spectral region (50 000 $-$70 000 cm^{-1}) is reported. Using energy-level calculations, all observed spectral lines could be assigned to free-ion term symbols (including term symbols with unusually high L and J, e.g., a $^2Q_{23/2}$ level around 67 000 cm^{-1}). From the ^6G_J levels around 50 000 cm^{-1} quantum cutting (or two-photon luminescence, photon-cascade emission) is observed: the emission of a red photon due to the $^6G_J \rightarrow {}^6P_J$ transition is followed by the emission of an ultraviolet photon due to the $^6P_J \rightarrow {}^8S_{7/2}$ transition.
[S0163-1829(97)01646-9]

I. INTRODUCTION

In the past decades experimental and theoretical work by scientists like Dieke,[1] Carnall *et al.*,[2] and many others has provided an overview of the $4f^n$ energy levels of all rare-earth ions in the infrared, visible, and ultraviolet spectral region. Energy-level calculations up to 50 000 cm^{-1} have been performed for all rare-earth ions and most of the energy levels have been observed experimentally.

In spite of the large number of papers on $4f^n$ energy levels of rare-earth ions, reports on $4f^n$ energy levels in the vacuum-ultraviolet spectral region (VUV; $E>50\,000$ cm^{-1}, $\lambda<200$ nm) are scarce. For the strong parity allowed $4f^n \rightarrow 4f^{n-1}5d$ transitions on the other hand, the spectra in the VUV region have been studied for most rare-earth ions in LaF_3, CaF_2, and $LiYF_4$, starting with the pioneering work by the group of Yen.[3,4] Only for a few rare-earth elements some $4f^n$ levels in the VUV have been calculated and/or observed.[5–9] One can think of two reasons for this lack of effort in the VUV region on $4f^n \rightarrow 4f^n$ transitions: (1) It is difficult. Measurements on the weak (parity forbidden) intraconfigurational $4f^n \rightarrow 4f^n$ transitions require special setups for luminescence spectroscopy in the VUV and calculations including levels above 50 000 cm^{-1} require larger matrices. Furthermore, the measurements on the $4f^n \rightarrow 4f^n$ transitions can be complicated by the difficulty of discriminating them from parity-allowed $4f^n \rightarrow 4f^{n-1}\ n'l$ background bands. Two-photon absorption spectroscopy has been used successfully to overcome this problem,[10] but to date this has not been extended into the VUV. (2) There are no applications that require knowledge on the $4f^n$ levels of rare-earth ions in the VUV.

The latter point has changed recently. The development of phosphors for excitation in the VUV has become an important new challenge in the field of luminescent materials research. VUV phosphors are required for application in mercury-free fluorescent tubes and in plasma display panels. In these devices a noble-gas discharge generates VUV radiation. The xenon dimer discharge, which yields a broad band in the VUV with the maximum at 172 nm (xenon dimer), gives the highest efficiency of all noble gases, but it is still less efficient than the conventional mercury discharge. The phosphors used in mercury discharge fluorescent tubes have quantum efficiencies close to 100%. Therefore, to make a mercury-free fluorescent tube competitive, a phosphor with a quantum efficiency higher than 100% is required. In other words, more than one visible photon should be obtained per absorbed VUV photon. One of the challenges is to find such a VUV phosphor, a so-called quantum cutter. The high energy of the VUV photons from a xenon dimer discharge makes it possible (in theory) to obtain quantum cutting (or two-photon luminescence, photon-cascade emission) in the visible. For rare-earth ions the phenomenon of quantum cutting is known,[11,12] but based on the current knowledge no efficient quantum cutter in the visible is possible.[13]

Our research program on finding an efficient quantum cutter involves three stages. First, the energy levels in the VUV region will be resolved for a number of rare-earth ions. Next, it will be investigated if efficient visible quantum cutting from one of the VUV levels is possible. Finally, promising ions will be incorporated in various host lattices to find a stable VUV phosphor with a high (close to 200%) quantum efficiency in the visible. The first ions to be investigated will be those ions that are able to give an efficient emission in the visible, either directly or after energy transfer, e.g., Sm^{3+}, Eu^{3+}, Gd^{3+}, Ho^{3+}, and Er^{3+}. To resolve the energy levels in the VUV region the lanthanides are incorporated in fluoride lattices (e.g., $LiYF_4$ and LaF_3). In these host lattices the opposite parity states ($4f^{n-1}5d$ and charge transfer) that can interfere with the energy levels of the $4f^n$ configuration are at the highest possible energies.

To investigate if efficient quantum cutting in the visible can be achieved, the emission spectra under VUV excitation will be analyzed. For efficient quantum cutting in the visible two conditions must be fulfilled. First, to get emission from a high-lying energy level, the gap to the next lower level should be large enough to prevent multiphonon relaxation.[14] Second, the branching ratio (i.e., the way the total emission intensity is divided over the various transitions in the IR, visible, and UV spectral region) must be appropriate. This

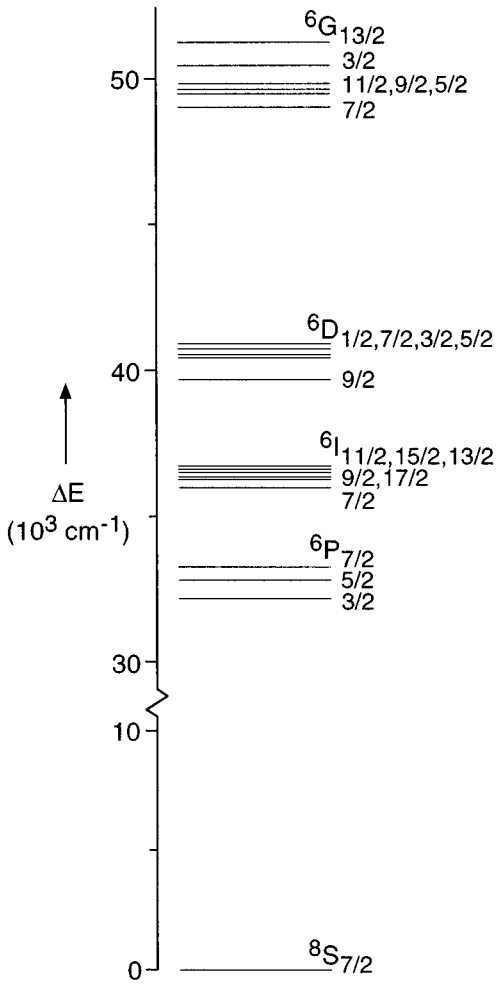

FIG. 1. Energy-level scheme in the range $0-50\,000\ \mathrm{cm}^{-1}$ for Gd^{3+} in fluoride lattices (Ref. 2). Note the break in the energy scale.

will be determined experimentally. With the aid of Judd-Ofelt theory the theoretical maximum quantum efficiency in the visible region can be calculated.

In this paper the results on Gd^{3+} in $LiYF_4$ are presented. The schematic energy-level diagram of Gd^{3+} $(4f^7)$ as far as it was known up until now is given in Fig. 1.[2] Every free-ion level ($^{2S+1}L_J$), which is denoted by a single horizontal bar, is in reality split into several Stark levels by the crystal field. In the first part of the paper the excitation spectrum in the region $50\,000-80\,000\ \mathrm{cm}^{-1}$ is reported. An overview of the positions of energy levels in the VUV spectral region is presented and compared with energy-level calculations performed for Gd^{3+}. The second part of the paper discusses quantum cutting for Gd^{3+}. Up until now, only emission to the $^8S_{7/2}$ ground state has been reported for Gd^{3+}, including the $^6G_J \rightarrow {}^8S_{7/2}$ emission around 200 nm, which has been found in several host lattices.[15] These emissions are all in the ultraviolet region. However, on the basis of the energy-level scheme of Gd^{3+} one can expect a visible emission in the orange/red due to the $^6G_J \rightarrow {}^6P_J$ transition, followed by emission of a second photon from the ^6P_J level. It will be shown that quantum cutting and visible emission can indeed be observed for Gd^{3+} in $LiYF_4$.

II. EXPERIMENTAL

A single crystal of $LiYF_4$:Gd^{3+} was grown using the Bridgman method. The crystal-growth melt contained 5 mol % of Gd^{3+}. The crystal was grown in a vitreous carbon crucible in a nitrogen atmosphere using a Philips PH 1006/13 high-frequency furnace. To obtain a crystal free of oxides, the crystal-growth chamber was flushed for several minutes with SF_6.[16] By this method a 4 cm-long crystal with a 1.5 cm diameter was obtained. A polished, transparent piece of 2 mm thick was used for the measurements. The powder sample of $LiGdF_4$:Eu^{3+} was prepared by firing stoichiometric mixtures of LiF, GdF_3, and EuF_3 at 550 °C in a nitrogen atmosphere. The samples were checked by x-ray-diffraction analysis and found to be single phase. $LiYF_4$ and $LiGdF_4$ have the inverse scheelite structure, space group $I4_1/a$. The site symmetry for the lanthanide ion is S_4.[17]

For low resolution spectroscopic measurements with excitation in the VUV, a Spex 1680 spectrofluorometer equipped with 0.22 m double monochromators was adapted for VUV measurements.[18] The excitation source was a D_2-lamp (Hamamatsu L1835, 150 W) fitted with a MgF_2 window. The light was focused by two MgF_2 lenses on the entrance slit of the excitation monochromator, which contained VUV coated gratings blazed at 150 nm (1200 g/mm) and Al mirrors coated with MgF_2 (ARC 1600). The emission monochromator was equipped with gratings blazed at 500 nm (1200 g/mm). The signal was detected with a cooled Hamamatsu R928 photomultiplier tube. The sample position could be optimized in all directions. The spectral resolution of this apparatus was approximately 0.5 nm. Before recording the spectra, the D_2-lamp housing, excitation monochromator, and sample compartment were flushed for at least 15 h with dry N_2 to remove air. By this method, excitation spectra could be recorded in the region 150–350 nm and emission could be measured in the region 250–800 nm. Excitation spectra were corrected for the lamp intensity and the transmission of the excitation monochromator by using sodium salicylate as a standard (the absorption and quantum efficiency are assumed to be constant in the energy range investigated).[19] All low resolution measurements were performed at room temperature.

The high resolution excitation measurements were carried out using synchrotron radiation and the equipment of the HIGITI experimental station[20] of the Synchrotronstrahlungslabor HASYLAB at DESY, Hamburg (Germany). All low-temperature spectra and emission spectra in the VUV region were also recorded with this experimental setup. The HIGITI experimental station is situated at the DORIS storage ring and a wiggler is used to enhance the beam intensity to 10^{13} photons/(sec mrad^2 0.1% bandwidth) (energy range 5–30 eV). The excitation light was dispersed through a 1 m Wadsworth monochromator with a holographic MgF_2-coated Al grating blazed at 150 nm (1200 g/mm). An estimated photon flux of 10^{11} photons/(Å sec) was obtained at the sample. The ultimate spectral resolution was about 0.3 Å. The area of the beam spot at the sample was less than 1 mm^2. The pressure in the monochromator and the sample chamber was maintained below 10^{-8} mbar. The temperature of the sample could be varied between liquid helium and room temperature. The emission could be measured in dif-

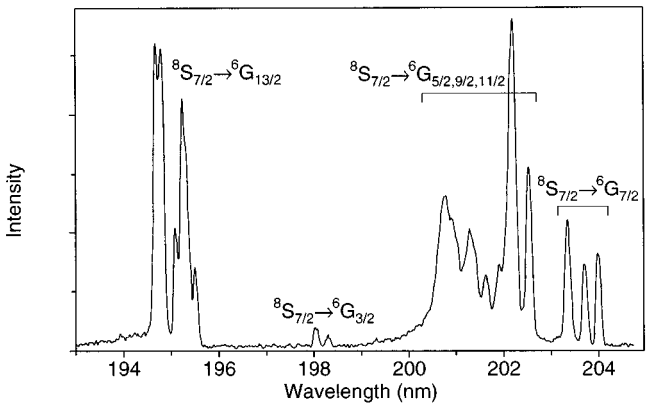

FIG. 2. $^8S_{7/2}\rightarrow{}^6G_J$ excitation spectrum of $LiYF_4$:Gd^{3+} 5% monitoring $^6P_{7/2}\rightarrow{}^8S_{7/2}$ emission (311.0 nm) at 9 K.

ferent ways, depending on the emission wavelength. For the region 300–700 nm a 0.2 m monochromator (Acton Research Corporation VM502; 600 g/mm) with a cooled Hamamatsu R943-02 photomultiplier tube was used. The light was guided from the sample chamber to the entrance slit of the monochromator by an optical fiber. VUV/UV emission was detected using a Hamamatsu 1645U-09 Channelplate detector attached to a 0.4 m Seya-Namioka monochromator with a holographic Al-MgF_2 grating blazed at 150 nm (1200 g/mm). The spectral resolution of both detection systems is >1 nm.

III. VACUUM-ULTRAVIOLET SPECTROSCOPY

In Fig. 2 the $^8S_{7/2}\rightarrow{}^6G_J$ excitation spectrum of $LiYF_4$:Gd^{3+} monitoring $^6P_{7/2}\rightarrow{}^8S_{7/2}$ emission (311.0 nm) at 9 K is shown. The spectral resolution was limited to 1 Å due to the relatively low intensity of $4f$-$4f$ transitions. The positions of all lines measured are tabulated in Table I. The lines correspond to transitions to various Stark levels of ^6G_J terms. The observation of these lines is not unique. Absorption spectra for LaF_3:Gd^{3+} down to 200 nm have been reported previously by Carnall *et al.*[2] Energy-level calculations by Carnall *et al.* for the ^6G_J levels for Gd^{3+} in LaF_3 are included in Table I for comparison. The agreement between the calculations for Gd^{3+} in LaF_3 and the presently observed levels for Gd^{3+} in $LiYF_4$ is good, considering the fact that Gd^{3+} is incorporated in different host lattices. For Gd^{3+} in $LiYF_4$ the barycenters of the $^6G_{7/2}$, $^6G_{3/2}$, and $^6G_{13/2}$ multiplets are 98, 70, and 140 cm^{-1} lower in energy, respectively. The crystal-field splittings for these multiplets are, on average, larger for $LiYF_4$:Gd^{3+} than for LaF_3:Gd^{3+}. Both observations are in agreement with what can be expected for Gd^{3+} on a smaller site [$r_{Y^{3+}}(\mathrm{VIII})=1.02$ Å, $r_{La^{3+}}(\mathrm{IX})=1.22$ Å].[21] Free-ion levels shift to lower energies for rare-earth ions substituted on smaller sites due to a slight decrease in electron repulsion (increase in overlap with ligand orbitals). The crystal-field splitting is well known to increase with decreasing ion-ligand separations. The number of Stark levels for every multiplet (Table I, last column) is equal for $LiYF_4$ and LaF_3. This is due to the relatively low site symmetry for the rare-earth ion in both lattices (S_4 and C_2, respectively), which means that all degeneracy is lifted by the crystal field except Kramers' degeneracy. It was not possible to perform energy-level calculations for $LiYF_4$:Gd^{3+} because the energy-level parameters needed have never been determined.

TABLE I. Experimentally observed ^6G_J energy levels for Gd^{3+} in $LiYF_4$, compared with calculated energy levels for Gd^{3+} in LaF_3 (Ref. 2). The last column gives the theoretical number of Stark levels for every ^6G_J term.

E_{exp} (cm^{-1}) ($LiYF_4$)	Multiplet	E_{calc} (cm^{-1}) (LaF_3)	No. of levels
49022	$^6G_{7/2}$	49160	4
49087		49225	
49174		49243	
~49236[a]		49284	
49373	$^6G_{11/2}$	49545	6
49456	$^6G_{9/2}$		5
49529	$^6G_{5/2}$		3
49596			
49680			
49766			
49811		49860	
50431	$^6G_{3/2}$	50486	2
50500		50568	
51148	$^6G_{13/2}$	51310	7
51190		51357	
51216		51382	
51261		51402	
51337		51414	
51369		51436	
		51483	

[a]This value is determined from the $^6G_J\rightarrow{}^6P_J$ emission spectrum of $LiYF_4$:Gd^{3+} in Fig. 5 (see text).

From Table I follows that for the $^6G_{7/2}$, $^6G_{3/2}$, and $^6G_{13/2}$ multiplets almost all Stark levels were found experimentally. The lines between 49 300 and 49 900 cm^{-1}, which correspond to $^8S_{7/2}\rightarrow{}^6G_{11/2}$, $^8S_{7/2}\rightarrow{}^6G_{9/2}$, and $^8S_{7/2}\rightarrow{}^6G_{5/2}$ transitions, cannot be assigned unambiguously. The multiplets $^6G_{11/2}$, $^6G_{9/2}$, and $^6G_{5/2}$ are too close in energy to distinguish and assign all overlapping Stark levels. Another reason for missing energy levels in the excitation spectrum can be a very low transition probability.

Figure 3 shows the excitation spectrum in the region 140–200 nm of $LiYF_4$:Gd^{3+} monitoring $^6P_{7/2}\rightarrow{}^8S_{7/2}$ emission at 9 K. The $^8S_{7/2}\rightarrow{}^6G_{13/2}$ lines are included to be able to compare the intensities in Fig. 3 with the $^8S_{7/2}\rightarrow{}^6G_J$ excitation spectrum in Fig. 2. In the spectrum, 40 lines due to $4f$-$4f$ transitions could be observed, which have not been observed or calculated before. The corresponding energies are given in Table II. In order to assign these lines, we performed energy-level calculations with the matrix-diagonalization and least-squares-refinement program REEL.[22] The parameters for Gd^{3+} in LaF_3 from Ref. 2 were used since the parameters for Gd^{3+} in $LiYF_4$ are not known. As was shown above, a small shift (some 100 cm^{-1}) to lower energies is expected for the free-ion levels of Gd^{3+} in $LiYF_4$ in comparison to Gd^{3+} in LaF_3. The parameters used are given in Table III. Only free-

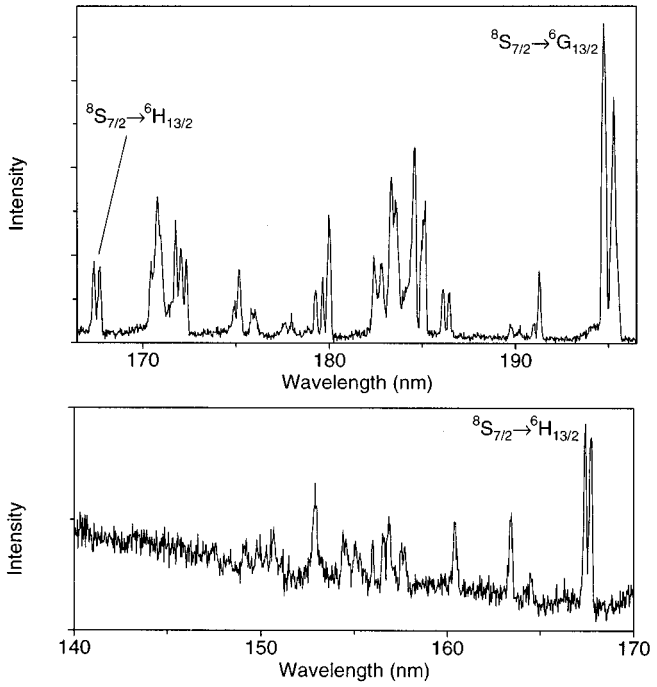

FIG. 3. VUV excitation spectrum of $LiYF_4$:Gd^{3+} 5% monitoring $^6P_{7/2}\rightarrow{}^8S_{7/2}$ emission (311.0 nm) at 9 K. The spectrum is split into two parts to make all lines visible. The $^8S_{7/2}\rightarrow{}^6H_{13/2}$ lines at 168 nm are present in both parts for intensity comparison. For assignments, see Table II.

ion parameters were used, in other words, the crystal-field parameters $B_q^{(k)}$ were kept zero. In this way for every $^{2S+1}L_J$ multiplet the barycenter of the Stark levels was obtained. The resulting free-ion energy levels are shown in Table II. The crystal field was not taken into account in the calculations since the energy differences between several free-ion levels are small. As a consequence, most of the single lines or groups of lines can only be assigned to a group of $^{2S+1}L_J$ multiplets (denoted in Table II by {}).

All calculated energy levels are assigned to $^{2S+1}L_J$ terms. One has to realize that for most multiplets in this high-energy region, mixing of several $^{2S+1}L_J$ terms (mostly with same J) is important. For example, the term that has the largest contribution in the free-ion level calculated at 55 732 cm^{-1} is $^6G_{9/2}$, but the terms $^4H(3)_{9/2}$ and $^4H(2)_{9/2}$ also have a large contribution. The consequence of mixing of the levels is that in some cases the same $^{2S+1}L_J$ term has the largest contribution in two different calculated levels. This is the reason that some $^{2S+1}L_J$ values, which are marked by an asterisk in Table II, occur twice in the assignments.

The highest-energetic excitation line measured (at 67 024 cm^{-1}) can be assigned to the transition to the $^2Q_{23/2}$ multiplet. To our knowledge, this is the first observation of an ion in a Q state, which corresponds to a total orbital quantum number L equal to 12. This extraordinarily high value of L can only be obtained for ions with f^6, f^7, or f^8 configuration. Values higher than 12 are not possible for intraconfigurational states.

The number of observed excitation lines in Fig. 3 is only a small fraction of the total number of theoretically expected energy levels in this region, which is the sum of the numbers

TABLE II. Experimentally observed energy levels in the range 52 000–67 500 cm^{-1} for Gd^{3+} in $LiYF_4$, compared with calculated free-ion energy levels for Gd^{3+} in LaF_3. The last column gives the theoretical number of Stark levels for every $^{2S+1}L_J$ term. The asterisks mark $^{2S+1}L_J$ terms which occur twice (for explanation, see text).

E_{exp} (cm^{-1}) ($LiYF_4$)	Multiplet	E_{calc} (cm^{-1}) (LaF_3)	No. of levels
52 277	$^6G_{7/2}$*	52 420	4
52 351			
52 554			
52 706	$^6F_{1/2}$	52 719	1
53 631	$^6F_{3/2}$	53 779	2
53 717			
54 002	$^6F_{11/2}$	54 277	6
54 168	$^6G_{5/2}$*	54 353	3
54 330	$^6F_{9/2}$	54 552	5
54 475	$^6F_{5/2}$	54 687	3
54 546	$^6F_{7/2}$	54 745	4
54 693			
54 822			
55 559	$^6G_{9/2}$*	55 732	5
55 661	$^4N_{17/2}$	55 862	9
55 779			
56 189	$^4H(2)_{7/2}$	56 220	4
56 300	$^4D(6)_{3/2}$	56 252	2
56 808	$^4H(2)_{13/2}$	56 945	7
56 880	$^4N_{19/2}$	57 061	10
57 091	$^6H_{5/2}$	57 169	3
57 162	$^4D(6)_{1/2}$	57 183	1
	$^4N_{23/2}$	57 329	12
	$^4H(2)_{11/2}$	57 451	6
	$^4N_{21/2}$	57 606	11
58 018	$^6H_{15/2}$	58 139	8
58 119	$^6H_{7/2}$	58 140	4
58 214	$^4L(2)_{13/2}$	58 254	7
58 551	$^4L(2)_{17/2}$*	58 298	9
58 665	$^4L(2)_{15/2}$	58 323	8
	$^6H_{11/2}$	58 577	6
	$^6H_{9/2}$	58 632	5
59 613	$^6H_{13/2}$	59676	7
59 730			
	$^4L(2)_{19/2}$	60 172	10
	$^4K(1)_{11/2}$	60 242	6
60 794	$^4F(4)_{9/2}$	60 831	5
61 181	$^4F(4)_{7/2}$*	61 204	4
62 348	$^4F(4)_{5/2}$	62 389	3
	$^4L(2)_{17/2}$*	62 536	9
	$^4K(1)_{13/2}$	62 721	7
	$^4K(1)_{15/2}$	62 900	8
63 437	$^4H(4)_{11/2}$	63 432	6
63 743	$^4H(4)_{9/2}$	63 703	5
63 881	$^4H(4)_{7/2}$	63 747	4
64 103	$^4G(6)_{5/2}$	63 938	3
	$^4F(4)_{3/2}$	63 981	2
	$^4S(2)_{3/2}$	64 210	2
64 392	$^4H(4)_{13/2}$	64 521	7
64 487	$^4G(5)_{11/2}$	64 595	6
64 746	$^4G(6)_{9/2}$	64 710	5
	$^4G(6)_{7/2}$	65 266	4
65 402	$^4I(4)_{11/2}$*	65 384	6
	$^4G(5)_{9/2}$	65 462	5
	$^4I(4)_{13/2}$	65 984	7
	$^4I(4)_{11/2}$*	66 225	6
66 366	$^4I(4)_{9/2}$	66 313	5
66 529	$^4G(5)_{5/2}$	66 425	3
66 720	$^4I(4)_{15/2}$	66 620	8
	$^4F(4)_{7/2}$*	66 910	4
67 024	$^2Q_{23/2}$	67 141	12
	$^2G(0)_{7/2}$	67 765	4

in the last column in Table II. This is due to the large number of $^{2S+1}L_J$ multiplets in a relatively small energy region, as already discussed. The resolution was too low to distinguish levels with an energy difference smaller than approximately 70 cm^{-1}, especially in the higher energy part of Fig. 3. As a result, in most cases the experimental excitation energies in Table II correspond to transitions to a number of levels rather than to one energy level.

Taking the considerations described above into account, the conclusion from the results in Table II is that the agreement between the experimental and calculated levels is good. The energy regions where excitation lines are found in Fig. 3 coincide with the energy regions where levels are calculated. In many cases the positions observed are 100–200 cm^{-1} lower than the calculated energies, which is in agreement with the shift to lower energy expected for Gd^{3+} in $LiYF_4$ in comparison to LaF_3.

For the scope of our research it is important that in the 150–200 nm region the maximum energy gap from a $4f$ level to the next lower level is approximately 1200 cm^{-1}. This means that in almost all host lattices, a Gd^{3+} ion excited in this region will decay nonradiatively by multiphonon relaxation to the ^6G_J levels around 200 nm.

A few $^{2S+1}L_J$ terms calculated in the 52 000–67 500 cm^{-1} region were not observed at all, apparently due to a too low transition probability. It should be mentioned that the Gd^{3+} $4f^7$ energy levels extend till above 150 000 cm^{-1},[23] although no $4f^7$-$4f^7$ transitions were observed above 67 500 cm^{-1} in our experiments. A possible explanation for this is the following. The multiphonon relaxation to the ^6G_J levels will involve an increasing number of steps for excitation at higher energies. At every step the multiphonon relaxation will have to compete with other processes like energy transfer to killer centers. Since the maximum energy gap between $4f$ levels in the VUV region is approximately 1200 cm^{-1}, the possibility for these other processes will generally be small compared to the probability for the multiphonon-relaxation process. However, if the number of steps in the nonradiative decay becomes large, the relative probability for the other processes will increase. This means that at high excitation energies the chance of reaching the ^6G_J levels via multiphonon relaxation can become very small. This could explain why we did not observe any $4f^7$-$4f^7$ transitions above 67 500 cm^{-1} in excitation measurements. This hypothesis could be verified by absorption or reflection spectroscopy, in which relaxation processes do not play a role. Note that in Fig. 3 an overall trend of decreasing intensity of the $4f^7$-$4f^7$ transitions with increasing excitation energy can be observed, which supports our explanation for the absence of $4f^7$-$4f^7$ lines in the excitation spectrum above 67 500 cm^{-1}.

TABLE III. Free-ion parameters for Gd^{3+} in LaF_3 (Ref. 2) used for the calculations in Table II.

Parameter	Value (in cm^{-1})
Electron repulsion	
F^2	85 669
F^4	60 825
F^6	44 776
Spin-orbit coupling	
ζ	1508
Two-body interaction	
α	18.92
β	−600
γ	1575
Three-body interaction	
T^2	300
T^3	42
T^4	62
T^6	−295
T^7	350
T^8	310

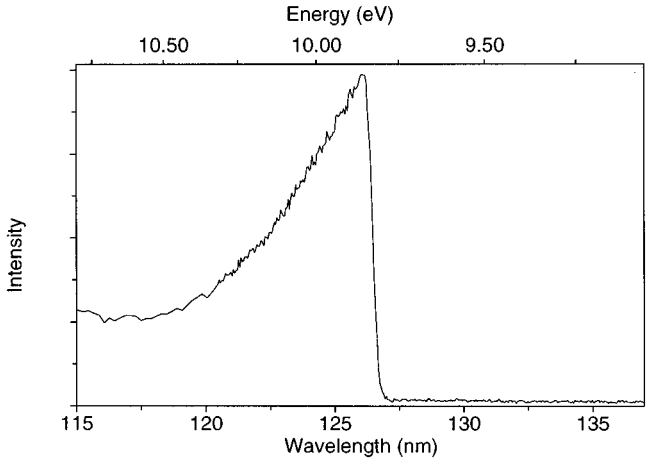

FIG. 4. VUV excitation spectrum of $LiYF_4$:Gd^{3+} 5% monitoring $^6P_{7/2} \rightarrow {}^8S_{7/2}$ emission (311.0 nm) at 9 K.

In a preliminary paper[24] we presented an excitation spectrum of $LiYF_4$:Gd^{3+} measured on the spectrofluorometer described in Sec. II, but without flushing with N_2. Peaks observed at 190.6, 189.2, and 187.2 nm were erroneously assigned to $4f$-$4f$ transitions on Gd^{3+}. We now know that the structure in this region of the spectrum is due to the absorption of the excitation light by oxygen.[25]

In Fig. 4 the excitation spectrum of $LiYF_4$:Gd^{3+} in the 115–135 nm region monitoring $^6P_{7/2} \rightarrow {}^8S_{7/2}$ emission at 9 K is given. The excitation band with a sharp edge at 127 nm is assigned to host-lattice absorption. The band has a high intensity relative to the $4f$-$4f$ transitions in Figs. 2 and 3. The assignment is based on the fact that for a number of trivalent rare-earth ions in $LiYF_4$ a strong excitation band around 120 nm was found, which was assigned to host-lattice absorption.[26] The steep onset is typical for band-gap excitation. The decrease of the intensity for energies higher than 9.85 eV (see Fig. 4) is explained as follows: because the optical density is very high at higher energies, the excitation light is absorbed near the surface of the crystal, where the concentration of killer sites is relatively high. Therefore the excitation energy is lost as a result of nonradiative processes.[27] In addition, the increase in absorption coefficient will result in a higher dielectric constant and thus a higher reflectivity. This effect will also contribute to the observed decrease in the excitation spectrum.

From the spectrum in Fig. 4 the band gap of $LiYF_4$ was

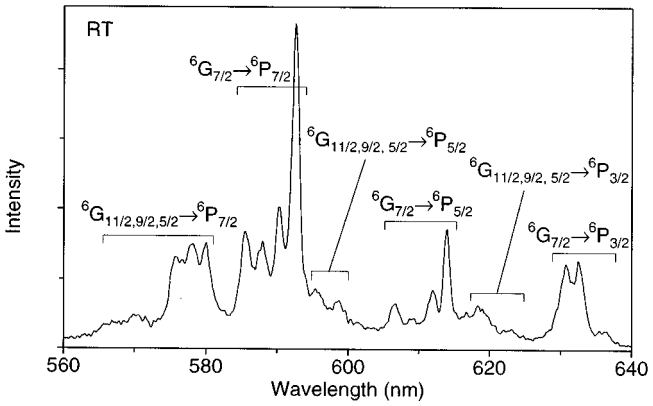

FIG. 5. $^6G_J\rightarrow{}^6P_J$ emission spectrum of $LiYF_4$:Gd^{3+} 5% upon $^8S_{7/2}\rightarrow{}^6G_J$ excitation (202.1 nm) at 300 K.

determined at 9.8 eV. An excitation spectrum in this region was also recorded at room temperature, resulting in a small shift of the band gap to 9.7 eV and a slight broadening of the edge. The temperature dependence of the energy gap is well known for semiconductors and is explained by thermal expansion of the lattice and temperature dependence of the phonon distribution.[28]

IV. QUANTUM CUTTING

The energy-level scheme in Fig. 1 shows the possibilities for quantum cutting in Gd^{3+}. The gap between the $^6G_{7/2}$ level and the next lower ^6D_J levels is large (8000 cm^{-1}) and therefore the multiphonon-relaxation rate will be negligibly small. Quantum cutting can occur when a Gd^{3+} ion excited in the ^6G_J levels returns to the ground state by two subsequent radiative transitions, e.g., $^6G_J\rightarrow{}^6P_J$ and $^6P_J\rightarrow{}^8S_{7/2}$. The $^6G_J\rightarrow{}^6P_J$ transitions are expected in the orange/red spectral region.

Figures 5 and 6 show the emission spectra of $LiYF_4$:Gd^{3+} in the visible upon excitation in the ^6G_J levels at room temperature and 9 K, respectively. Indeed, emission is observed around 600 nm. All emission lines in these spectra are assigned to $^6G_J\rightarrow{}^6P_J$ transitions of Gd^{3+}. The energies of the emission lines agree very well with the calculated differences between the energies of the measured ^6G_J levels (Table I)

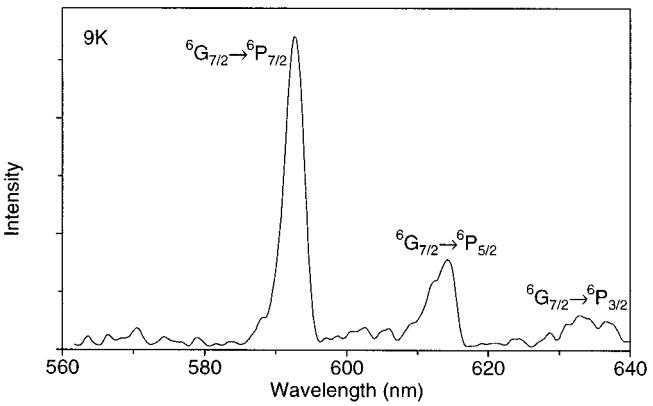

FIG. 6. $^6G_{7/2}\rightarrow{}^6P_J$ emission spectrum of $LiYF_4$:Gd^{3+} 5% upon $^8S_{7/2}\rightarrow{}^6G_{13/2}$ excitation (194.7 nm) at 9 K.

TABLE IV. Assignment of the $^6G_J\rightarrow{}^6P_J$ emission lines for Gd^{3+} in $LiYF_4$ from Fig. 5. The numbers in parentheses correspond to measured Stark levels.

E_{exp} (cm^{-1})	Transition
15 721	$^6G_{7/2}(1)\rightarrow{}^6P_{3/2}$
15 810	$^6G_{7/2}(2)\rightarrow{}^6P_{3/2}$
15 855	$^6G_{7/2}(3)\rightarrow{}^6P_{3/2}$
16 046	$^6G_{11/2,9/2,5/2}(1)\rightarrow{}^6P_{3/2}$
16 100–16 240	$^6G_{11/2,9/2,5/2}(>)\rightarrow{}^6P_{3/2}$
16 287	$^6G_{7/2}(1)\rightarrow{}^6P_{5/2}$
16 340	$^6G_{7/2}(2)\rightarrow{}^6P_{5/2}$
16 418	$^6G_{7/2}(3)\rightarrow{}^6P_{5/2}$
16 480	$^6G_{7/2}(4)\rightarrow{}^6P_{5/2}$
16 700	$^6G_{11/2,9/2,5/2}(2)\rightarrow{}^6P_{5/2}$
16 740–16 820	$^6G_{11/2,9/2,5/2}(>)\rightarrow{}^6P_{5/2}$
16 872	$^6G_{7/2}(1)\rightarrow{}^6P_{7/2}$
16 938	$^6G_{7/2}(2)\rightarrow{}^6P_{7/2}$
17 010	$^6G_{7/2}(3)\rightarrow{}^6P_{7/2}$
17 077	$^6G_{7/2}(4)\rightarrow{}^6P_{7/2}$
17 238	$^6G_{11/2,9/2,5/2}(1)\rightarrow{}^6P_{7/2}$
17 298	$^6G_{11/2,9/2,5/2}(2)\rightarrow{}^6P_{7/2}$
17 361	$^6G_{11/2,9/2,5/2}(>)\rightarrow{}^6P_{7/2}$
17 480–17 690	$^6G_{11/2,9/2,5/2}(>)\rightarrow{}^6P_{7/2}$

and the energies of the ^6P_J levels for $LiYF_4$:Gd^{3+} from Ref. 29. As far as we are aware, this is the first observation of visible luminescence from Gd^{3+}.

The low-temperature emission spectrum (Fig. 6), which was recorded at the DESY synchrotron (see Sec. II), shows three lines at 592.7, 614.0, and 636.1 nm. These are assigned to the emissions from the lowest $^6G_{7/2}$ level to the $^6P_{7/2}$, $^6P_{5/2}$, and $^6P_{3/2}$ multiplets, respectively. The resolution of the emission monochromator was too low to resolve the emissions to the different Stark levels of the ^6P_J multiplets, which differ only a few tens of cm^{-1} in position.[29]

All emission lines measured in the room-temperature spectrum (Fig. 5), recorded on the modified spectrofluorometer (see Sec. II), and their assignments are tabulated in Table IV. As expected, the three lines observed in the low-temperature emission spectrum are present at the same position and with the same intensity ratio, although the linewidths are much smaller. This is due to the better resolution of the emission monochromator compared to that at the DESY synchrotron. At the high-energy side of these three lines new emission lines show up at room temperature, which can be assigned to emissions from thermally populated higher $^6G_{7/2}$ and $^6G_{11/2,9/2,5/2}$ levels. Just as for the low-temperature spectrum, the spectral resolution of the monochromator was too low to resolve emissions to the different Stark levels of the ^6P_J multiplets. However, the energy differences between the $^6G_{7/2}$ Stark levels are larger than those between ^6P_J Stark levels. This resulted in the assignment of the emission lines to transitions from different $^6G_{7/2}$ Stark levels to ^6P_J multiplets. For every transition in Table IV a number is added in parentheses, which corresponds to the $^6G_{7/2}$ Stark level from which the emission originates. The numbers increase with increasing energy of the level. For emissions from the $^6G_{11/2,9/2,5/2}$ levels the same

is observed. Due to a low emission intensity and to the fact that only a few of these levels can be resolved in Fig. 2 because the energy differences are too small, it is difficult to distinguish different $^6G_{11/2,9/2,5/2} \rightarrow {}^6P_J$ emission lines. Therefore, some weak emissions in Fig. 5 are assigned to transitions from a number of higher energetic $^6G_{11/2,9/2,5/2}$ levels to a ^6P_J multiplet. This is denoted in Table IV by (>).

The assignments of the lines at 585.6 and 606.8 nm (17 077 and 16 480 cm^{-1}, respectively) to emissions from the $^6G_{7/2}(4)$ level is not based on calculated differences between the energies of measured levels, because the $^6G_{7/2}(4)$ level was not observed in the excitation spectrum (Fig. 2). We assign these emissions on the basis of the following. For $^6G_{7/2} \rightarrow {}^6P_{7/2}$ as well as $^6G_{7/2} \rightarrow {}^6P_{5/2}$ four lines are found, from which the three lowest energetic can be assigned to emissions from the three $^6G_{7/2}$ Stark levels determined from Fig. 2. The energy difference between the highest energetic emission line and the other three is approximately the same for both $^6G_{7/2} \rightarrow {}^6P_{7/2}$ and $^6G_{7/2} \rightarrow {}^6P_{5/2}$. Therefore the two lines mentioned above are assigned to emissions from the $^6G_{7/2}(4)$ level. The energy for this level determined from the emission spectrum is included in Table I. The fact that the $^8S_{7/2} \rightarrow {}^6G_{7/2}(4)$ excitation is not observed in the spectrum in Fig. 2 is likely due to a too low transition probability.

The assignments of the $^6G_J \rightarrow {}^6P_J$ emission lines differ from those in Ref. 24 because the setup used for those measurements was not properly calibrated in the VUV region. Moreover, only low-resolution spectra could be recorded, resulting in a higher inaccuracy in the positions of the ^6G_J levels.

To be able to assign the emission lines in the orange/red spectral region unambiguously to $^6G_J \rightarrow {}^6P_J$ emission from Gd^{3+}, the possibility of emission from other rare-earth ions that emit in this region has to be excluded. In Ref. 24 the possibility of Eu^{3+} emission at 590.6 and 614.0 nm (16 938 and 16 287 cm^{-1}, respectively) was suggested. Based on the present observations, all emission lines can be assigned to $^6G_J \rightarrow {}^6P_J$ transitions on Gd^{3+} and Eu^{3+} emission can be excluded: first, all emission positions agree very well with calculated positions for $^6G_J \rightarrow {}^6P_J$ lines. This is especially the case for the 614.0 nm line, which is also present in the 9 K emission spectrum (Fig. 6) and is as a consequence assigned to an emission from the lowest ^6G_J level. Next, there are more Eu^{3+} emission lines in this region (see Ref. 24), which are not present in Fig. 5. The clearest proof that the visible emission in Figs. 5 and 6 does not originate from Eu^{3+} is supplied by Fig. 7. In this figure the excitation spectra of $LiYF_4$:Gd^{3+} (trace *a*) and $LiGdF_4$:Eu^{3+} (trace *b*) are presented, both monitoring emission in the 590–593 nm range. For $LiGdF_4$:Eu^{3+} the monitored $^5D_0 \rightarrow {}^7F_1$ emission on Eu^{3+} occurs after energy transfer from the ^6P_J levels of Gd^{3+}, and therefore the $^8S_{7/2} \rightarrow {}^6I_J$, $^8S_{7/2} \rightarrow {}^6D_J$, and $^8S_{7/2} \rightarrow {}^6G_J$ transitions are present in the excitation spectrum. As can be seen in Fig. 7, trace *a*, for $LiYF_4$:Gd^{3+} the orange emission only occurs after excitation in the ^6G_J levels or higher. This shows that this emission is not originating from Eu^{3+}, but from the ^6G_J levels of Gd^{3+}.

Other rare-earth ions which could be present as impurities and give emission in the region around 600 nm are Tb^{3+}, Sm^{3+}, Dy^{3+}, and Ho^{3+}, but the spectral positions of the lines observed in Figs. 5 and 6 do not coincide with those of these ions in $LiYF_4$.

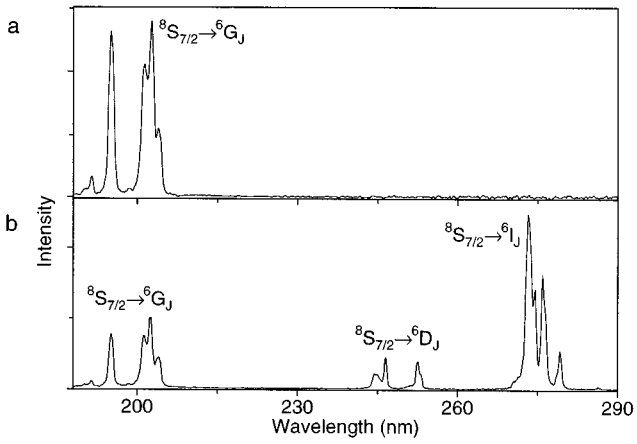

FIG. 7. (a) Excitation spectrum of $LiYF_4$:Gd^{3+} 5% monitoring $^6G_{7/2} \rightarrow {}^6P_{7/2}$ emission (592.7 nm) of Gd^{3+} at 300 K. (b) Excitation spectrum of $LiGdF_4$:Eu^{3+} 0.5% monitoring $^5D_0 \rightarrow {}^7F_1$ emission (590.7 nm) of Eu^{3+} at 300 K.

Upon $^8S_{7/2} \rightarrow {}^6G_J$ excitation quantum cutting occurs because the $^6G_J \rightarrow {}^6P_J$ emission is followed by the $^6P_J \rightarrow {}^8S_{7/2}$ emission. The visible quantum efficiency is low due to the following two factors. First, the second photon due to $^6P_J \rightarrow {}^8S_{7/2}$ emission of Gd^{3+} is situated around 311 nm, which is in the UV. Second, a Gd^{3+} ion has several possibilities to decay from the ^6G_J levels, of which the $^6G_J \rightarrow {}^6P_J$ transition is the only emission in the visible. Other emissions from the ^6G_J levels also occur, as can be seen in Fig. 8, which shows the UV emission spectrum of $LiYF_4$:Gd^{3+} upon excitation in the $^6G_{13/2}$ levels at room temperature. Around 204 nm the emission from the ^6G_J levels to the ground state is observed. The fact that the $^6I_J \rightarrow {}^8S_{7/2}$ emission around 278 nm is present in Fig. 8 shows that decay from the ^6G_J levels to the ^6I_J levels also takes place. Indeed, upon ^6G_J excitation the $^6G_J \rightarrow {}^6I_J$ emission is observed in the near infrared, viz. around 750 nm. The emission from the ^6I_J levels to the ground state is weak compared to the $^6P_J \rightarrow {}^8S_{7/2}$ emission. However, at room temperature the nonradiative transition probability of the $^6I_{7/2}$ levels of Gd^{3+}

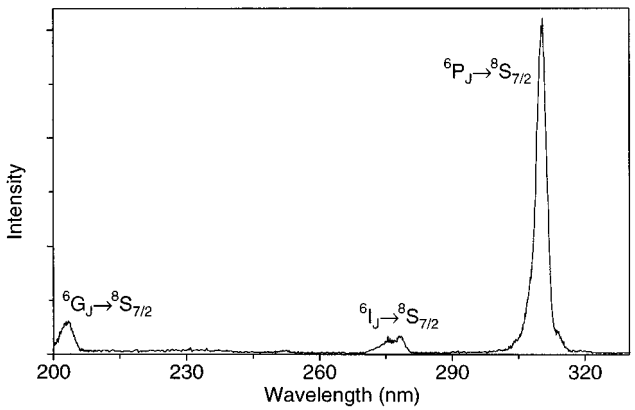

FIG. 8. UV emission spectrum of $LiYF_4$:Gd^{3+} 5% upon $^8S_{7/2} \rightarrow {}^6G_{13/2}$ excitation (194.7 nm) at 300 K.

in $LiYF_4$ to the $^6P_{5/2}$ levels is approximately 5 times larger than the $^6I_{7/2} \rightarrow {}^8S_{7/2}$ radiative transition probability.[30] The $^6I_J \rightarrow {}^6P_J$ nonradiative decay results in $^6P_J \rightarrow {}^8S_{7/2}$ emission. From this follows that almost half of the intensity of the $^6P_J \rightarrow {}^8S_{7/2}$ emission is due to decay via the ^6I_J levels.

From the discussion above it is clear that the branching ratio for the visible emission is not very favorable. No quantitative analysis could be performed because the spectrum in Fig. 8 could not be corrected for the instrumental response. Further, the $U^{(\lambda)}$ reduced matrix elements, which are required for a quantitative Judd-Ofelt analysis, have not been calculated for the transitions involving the ^6G_J term of Gd^{3+}.

Based on the results presented it can be concluded that an efficient quantum cutter in the visible based on Gd^{3+} alone is not possible. However, recently promising results have been obtained by a combination of Gd^{3+} and Eu^{3+} where two-step energy transfer from Gd^{3+} to Eu^{3+} (cross relaxation followed by direct energy transfer) yielded quantum efficiencies close to 200% in the red.[31,32]

V. CONCLUSIONS

In this paper an overview of $4f^n$ energy levels in the VUV spectral region for a rare-earth ion is presented. For Gd^{3+} in $LiYF_4$ a large number of $4f^7$ levels is observed at energies higher than 50 000 cm^{-1}. A good agreement with calculated free-ion energy levels is obtained. Upon excitation in the the ^6G_J levels around 200 nm quantum cutting occurs: the $^6G_J \rightarrow {}^6P_J$ emission, which is in the orange/red spectral region, is followed by the $^6P_J \rightarrow {}^8S_{7/2}$ UV emission. An efficient quantum cutter in the visible region based on Gd^{3+} alone is not possible.

ACKNOWLEDGMENTS

The authors are grateful to P. Gürtler from HASYLAB for the opportunity to use the excellent facilities for VUV spectroscopy at the DESY synchrotron, Hamburg (Germany), and to C. Ronda (Philips Research Laboratories, Aachen, Germany) for encouraging this research. The work described here was supported by the Netherlands Foundation for Chemical Research (SON), with financial aid from the Netherlands Organization for Scientific Research (NWO) and the Netherlands Foundation for Technical Research (STW).

*Corresponding author. FAX: +31 30 2532403; Electronic address: R.T.Wegh@fys.ruu.nl

[1] G. H. Dieke, *Spectra and Energy Levels of Rare Earth Ions in Crystals* (Interscience, New York, 1968).
[2] W. T. Carnall, G. L. Goodman, K. Rajnak and R. S. Rana, Argonne National Laboratory Report No. ANL-88-8, 1988 (unpublished).
[3] L. R. Elias, Wm. S. Heaps, and W. M. Yen, Phys. Rev. B **8**, 4989 (1973).
[4] Wm. S. Heaps, L. R. Elias, and W. M. Yen, Phys. Rev. B **13**, 94 (1976).
[5] W. T. Carnall, P. R. Fields, and R. Sarup, J. Chem. Phys. **57**, 43 (1972).
[6] A. A. Vlasenko, L. I. Devyatkova, O. N. Ivanova, V. V. Mikhailin, S. P. Chernov, T. V. Uvarova, and B. P. Sobolev, Sov. Phys. Dokl. **30**, 395 (1985).
[7] L. I. Devyatkova, O. N. Ivanova, V. V. Mikhailin, S. N. Rudnev, and S. P. Chernov, Opt. Spectrosc. (USSR) **62**, 275 (1987).
[8] K. M. Devyatkova, O. N. Ivanova, K. B. Seiranyan, S. A. Tamazyan, and S. P. Chernov, Sov. Phys. Dokl. **35**, 40 (1990).
[9] E. Sarantopoulou, A. C. Cefalas, M. A. Dubinskii, C. A. Nicolaides, R. Yu. Abdulsabirov, S. L. Korableva, A. K. Naumov, and V. V. Semashko, Opt. Commun. **107**, 104 (1994).
[10] M. C. Downer, C. D. Cordero-Montalvo, and H. Crosswhite, Phys. Rev. B **28**, 4931 (1983).
[11] J. L. Sommerdijk, A. Bril, and A. W. de Jager, J. Lumin. **8**, 341 (1974); **9**, 288 (1974).
[12] W. W. Piper, J. A. DeLuca, and F. S. Ham, J. Lumin. **8**, 344 (1974).
[13] R. Pappalardo, J. Lumin. **14**, 159 (1976).
[14] L. A. Riseberg and M. J. Weber, in *Progress in Optics XIV*, edited by E. Wolf (North-Holland, Amsterdam, 1976), p. 116.
[15] L. H. Brixner and G. Blasse, Chem. Phys. Lett. **157**, 283 (1989).
[16] M. Robinson, J. Cryst. Growth **75**, 184 (1986).
[17] R. E. Thoma, C. F. Weaver, H. A. Friedman, H. Insley, L. A. Harris, and H. A. Yakel, J. Phys. Chem. **65**, 1096 (1961).
[18] D. B. Johnston and S. Lipsky, J. Phys. Chem. **95**, 1896 (1991).
[19] J. A. R. Samson, *Techniques of Vacuum Ultraviolet Spectroscopy* (Wiley, New York, 1967), p. 212.
[20] U. Hahn, N. Schwentner, and G. Zimmerer, Nucl. Instrum. Methods **152**, 261 (1978).
[21] R. D. Shannon, Acta Crystallogr. A **32**, 751 (1976).
[22] P. Porcher (unpublished).
[23] G. H. Dieke and H. M. Crosswhite, Appl. Opt. **2**, 675 (1963).
[24] R. T. Wegh and A. Meijerink, Proceedings of the 2nd Winter Workshop on Spectroscopy and Structure of Rare Earth Systems, Polanica Zdrój, 1996 [Acta Phys. Pol. A **90**, 333 (1996)].
[25] A. N. Zaidel' and E. Ya. Shreider, *Vacuum Ultraviolet Spectroscopy* (Ann Arbor-Humprey Science, London, 1970), p. 280.
[26] K. H. Yang and J. A. DeLuca, Phys. Rev. B **17**, 4246 (1978).
[27] J. A. Groenink and G. Blasse, J. Solid State Chem. **32**, 9 (1980).
[28] N. W. Ashcroft and N. D. Mermin, *Solid State Physics* (Saunders, Philadelphia, 1976), p. 566.
[29] A. J. de Vries, M. F. Hazenkamp, and G. Blasse, J. Lumin. **42**, 275 (1988).
[30] J. Sytsma, G. F. Imbush, and G. Blasse, J. Phys. Condens. Matter **2**, 5171 (1990).
[31] H. Donker, R. T. Wegh, A. Meijerink, J. C. Krupa, and M. Queffelec, Proceedings of the Second International Conference on the Science and Technology of Display Phosphors [J. Soc. Information Display (to be published)].
[32] R. T. Wegh, H. Donker, and A. Meijerink (unpublished).